Energetic and vibrational analysis of hydrogenated silicon *m* vacancies above saturation

S. Alireza Ghasemi,[1,*] Thomas J. Lenosky,[2] Maximilian Amsler,[3] Ali Sadeghi,[3] Luigi Genovese,[4] and Stefan Goedecker[3]

[1]*Institute for Advanced Studies in Basic Sciences, P.O. Box 45195-1159, IR-Zanjan, Iran*

[2]*1974 Kirby Way, San Jose California 95124-1324, USA*

[3]*Department of Physics, Universität Basel, Klingelbergstr. 82, CH-4056 Basel, Switzerland*

[4]*Université Grenoble Alpes, CEA, INAC-SP2M, L_Sim, F-38000 Grenoble, France*

(Received 18 March 2014; revised manuscript received 11 August 2014; published 27 August 2014)

We present a systematic study on hydrogenated silicon *m* vacancies above saturation. For each system a global geometry optimization search for low-lying local minima is performed using a newly developed SiH tight binding model. Subsequently a large number of low-energy structures are examined by density functional calculations using a minimal basis set. Finally the energetically favorable structures are reexamined using a systematically extendable basis set with local, semilocal, and hybrid exchange-correlation functionals. Particular attention is paid to the divacancy to which the Raman peak at 3822 cm^{-1} associated with the H_2 molecule had previously been assigned. Both the energetics and vibrational analysis of divacancy-related stable configurations suggest a revision of the above conclusion.

DOI: 10.1103/PhysRevB.90.054117 PACS number(s): 61.72.jd, 46.15.−x, 78.55.Ap

I. INTRODUCTION

Hydrogen in semiconductors, particularly in silicon, is of great importance both industrially and scientifically. The interaction of hydrogen with defects in silicon, e.g., by passivating dangling bonds of silicon vacancies, affects the electronic structure of silicon systems, thereby reducing the electrical activity of point and extended defects [1]. By means of H^+ implantation and annealing, thin films of silicon can be exfoliated and formed on top of silicon wafers [2]. The fundamental phenomena that drive such a complicated hydrogen-induced process have been investigated previously [3,4]. However, some microscopic details like the role of microvoids and the onset of their development into the macroscopic cracks remains unclear. In addition, the role of hydrogen in different stages of this process warrants further investigation. A precise and complete study on the microscopic structures of hydrogenated silicon multivacancies is essential to address the above questions.

H atoms form strong bonds to Si atoms inside or in proximity of defects created either by Si^+ or H^+ implantation. In order to understand microscopic structures of such hydrogenated defects and molecular hydrogen in silicon, a number of experimental [3,5–8] and theoretical [9–14] studies have been reported. Three major vibrational frequencies associated with the stretching mode of H_2 molecules are observed in Raman scattering and infrared (IR) experiments. The Raman line at 4158 cm^{-1} [labeled as H_2(I)], which was initially observed by Murakami *et al.* [15] and subsequently by a number of other studies [16–21], is considered to be due to H_2 in plateletlike defects. Another, lower stretching mode of H_2 molecules at 3618 cm^{-1} [labeled as H_2(II)], which is observed both by use of IR [22–26] and Raman spectroscopy [16,18,19], is attributed to H_2 at the tetrahedral (T_d) interstitial site [17,27,28].

Since the first observation of a Raman line of H_2 at 3822 cm^{-1} [labeled as H_2(III)] in ion-implanted silicon followed by a hydrogen atom treatment [5], both experimental [3,6–8] and theoretical [9,10,12,29] studies have been performed to determine the microscopic structure of the trap which encompasses the hydrogen molecule. In the experiment by Ishioka and coworkers [5], the implanted samples were treated with atomic hydrogen at 250 °C for 3 h in a remote downstream of hydrogen plasma. This Raman line appears only for the silicon samples implanted with fluences between 1×10^{13} and 5×10^{14} Si^+/cm^2. Based on first principle calculations, Akiyama and Oshiyama presented possible microscopic structures of hydrogenated multivacancies in silicon [29]. Using calculated vibrational frequencies of the stretching modes of the trapped H_2 and Si-H units, they assigned the Raman peak at 3822 cm^{-1} to a trapped H_2 at a fully saturated hydrogenated divacancy.

Theoretical systematic investigations by Lee and coworkers [30] on microscopic structures of nonhydrogenated multivacancies showed that small defects thermodynamically exclusively favor fourfold coordination rather than hexagonal ringlike structure formation. In fact, simple approaches such as the dangling-bond counting model [31] and local relaxation [10,32,33] of intuitively constructed structures cannot predict the ground-state configurations of nonhydrogenated multivacancies. Similar to the strategy followed by Lee and coworkers, in this paper we perform a systematic search over stable configurations of hydrogenated silicon multivacancies.

II. METHODS

A. Calculation procedure

We perform a systematic study on the stable structures of hydrogenated silicon multivacancies using the minima hopping (MH) method [35] based on a SiH tight binding (TB) scheme (see Sec. II B) which is an extension of the Lenosky silicon TB [34]. The MH method is a global optimization method which can efficiently explore the low-lying regions of the energy landscape aiming at the global minimum [36]. Methods such as force fields typically result in an imperfect energy ordering and differences as well as a number of spurious minima [37]. This is true also for TB but to a much lesser extent

*aghasemi@iasbs.ac.ir

depending on the accuracy of the TB scheme employed as well as the fitting process. Therefore, an accurate identification of stable structures requires the use of more accurate methods such as density functional theory (DFT). In the case of multivacancies with many H atoms, there are many ways to arrange vacant sites and H atoms where all have low energies. Examining all these structures using DFT with a systematic basis is a formidable task. For this reason, the MH calculations are followed by DFT calculations with minimal basis sets using SIESTA [38]. In this way, a large number of configurations (about 500–1000) are examined with a higher level of theory. In the next step, the low-energy configurations obtained in SIESTA (about 20–100) are recalculated by pseudopotential DFT calculations using the BIGDFT code [39] which is based on a systematically extendable orthogonal wavelet basis set. Goedecker-type pseudopotentials are used [40]. In order to accurately identify the stable defects observed experimentally, our final calculations are carried out in the framework of DFT with a hybrid functional, namely PBE0.

A grid spacing of 0.4 Bohr is used in the BIGDFT calculations for representing the wave function. Each configuration is relaxed such that the maximum component of the force vector drops below 0.01 eV/Å. In order to ensure convergence with respect to supercell size and to avoid artifacts due to the interaction between the periodic images of the defect, all calculations, including global optimization, are performed with 216-atom supercells. This is particularly important for large vacancy clusters where interaction between the defect and its periodic images may not be negligible if smaller supercells were used. All results presented in this paper are calculated at the Γ point since our tests on a number of configurations showed that the inclusion of a 2×2×2 k-point mesh has only a small effect on total energy differences (about 10 meV).

Here we investigate multivacancies up to V_6. Dangling bonds of multivacancies V_n with $1 \leqslant n \leqslant 5$ can be fully passivated by $2n + 2$ H atoms. The hexavacancy V_6, which is a closed ring, requires only 12 H atoms instead of 14. Previous calculations by Akiyama [9,29] and our results show that the multivacancies readily absorb hydrogens up to full saturation (namely $2n + 2$ H atoms). In this way, the defected crystal remains at the original diamond structure with minimal strain. It is worth mentioning that m vacancy denotes a system in which there are m vacancies disregarding the configuration or arrangement of vacancies and we use the term multivacancies (also divacancy, trivacancy, etc.) for configurations in which vacancies cluster. In this paper we focus on hydrogenated silicon m vacancies with excess H atoms. More precisely, additional hydrogen molecule(s) are embedded into fully saturated silicon m vacancies. Our calculations are applicable to crystalline silicon bulk experiments in which large concentrations of H atoms have been incorporated by hydrogen treatment or by H^+ implantation.

B. Lenosky SiH tight binding

There has been some effort in developing SiH tight binding schemes. A number of parametrizations for different SiH tight binding schemes have been fitted to small molecules [41–46]. Recently, Bacalis *et al.* [47] developed a SiH tight binding model which was fitted to density functional results for nanocrystals with diameters up to 2.5 nm. A nonorthogonal tight binding scheme for Si and SiH systems was developed by Frauenheim *et al.* [48].

Based on the Lenosky tight binding scheme [34] for silicon, we fit new parameters for the Si-H and H-H interactions. The parameters are fitted to a DFT database which consists of hydrogenated silicon clusters: fully hydrogenated small molecules, partially and fully hydrogenated medium-size silicon clusters Si_nH_m ($n = 10,11,14$ and $m = 1,\ldots,16$). These structures are relaxed in DFT within LDA using the CPMD [49] code. Moreover, for each stable geometry, three structures are generated by randomly displacing atoms from equilibrium and added to the fitting database. The parameter optimizations are carried out using the least-squares method developed by Powell [50]. Table I shows the information necessary to construct the potential for Si-H and H-H interactions while the

TABLE I. The fitted parameters for Si-H and H-H tight binding. The Si-H tight binding is determined by three functions, $\Phi(r)$,$h_{ss\sigma}(r)$,$h_{sp\sigma}(r)$, and the H-H tight binding is determined by two functions, $\Phi(r)$,$h_{ss\sigma}(r)$. The onsite energy for the H atom is $\epsilon_H = 2.869732$ (eV). We have defined the functions $g_\alpha(r)$ by $h_\alpha(r) = (1/r^2)g_\alpha(r)$, where α stands for $ss\sigma$ or $sp\sigma$. The lower cutoff radius for the H-H interaction is $r_l = 0.39688$ Å. At distances smaller than r_l, the functions $g(r)$ are extrapolated linearly and the functions $\Phi(r)$ are extrapolated by fitting $(1/r)$ and $(1/r^2)$ terms to the values of $\Phi(r_l)$ and $\Phi'(r_l)$. The Si-Si parameters as well as the format of splines are as Ref. [34].

	Si-H			H-H	
r (Å)	$\Phi(r)$ (eV)	$g_{ss\sigma}(r)$ (Å^2 eV)	$g_{sp\sigma}(r)$ (Å^2 eV)	$\Phi(r)$ (eV)	$g_{ss\sigma}(r)$ (Å^2 eV)
0.39688	13.771593	−7.400876	4.047173	23.059179	−1.895939
1.20407	4.889563	−7.681206	4.318454	1.959504	−5.111052
2.01126	0.437630	−9.133024	5.607316	−0.082453	−4.235687
2.81844	0.070360	−2.579265	3.747888	−0.109054	−2.739931
3.62563	0.025676	−1.620682	−0.504652	0.013467	−3.629578
4.43281	0.055270	−9.582420	−2.404798	0.029248	−6.168522
5.24000	0.000000	0.000000	0.000000	0.000000	0.000000
r (Å)	$[\Phi(r)]'$ (Å^{-1} eV)	$[g_{ss\sigma}(r)]'$ (Å eV)	$[g_{sp\sigma}(r)]'$ (Å eV)	$[\Phi(r)]'$ (Å^{-1} eV)	$[g_{ss\sigma}(r)]'$ (Å eV)
0.39688	−0.587720	30.466775	−19.251201	−60.098689	−9.307944
5.24000	0.0	0.0	0.0	0.0	0.0

parameters for the Si-Si interaction are as in Ref. [34]. Our SiH parametrization has been previously used in several studies: simulation of silicon tips [51,52] in atomic force microscopy and high-pressure structures of disilane [53].

III. RESULTS

We calculate DFT energies using three different exchange-correlation functionals: LDA, PBE, and PBE0. Due to the various environments for H atoms among different configurations, the well-known self-interaction error may result in inaccurate energetics. It is known that PBE0 improves over conventional functionals for the self-interaction error and provides more accurate atomization energies for H-containing compounds. Therefore, we make our conclusions based on PBE0 energy values. Configurations in which vacancies are split, associated, closed rings are labeled as S, A, and A', respectively. Moreover, the superscripts in configuration labels denote the composition, e.g., $S_1^{p,q}$ is the first lowest energy S-type configuration of V_pH_q.

A. VH_6 (H_2@VH_4)

Removing one Si atom from bulk introduces four dangling bonds which can readily be passivated by H atoms provided that the H concentration in the vicinity of the vacancy is sufficiently large. Adding two extra H atoms to this fully H-decorated configuration results in a stable H_2 molecule close to the vacancy. The H_2 molecule is dislodged from the vacant site toward ⟨010⟩ by 2.55 Å. The orientation of the H_2 molecule is almost in the ⟨101⟩ direction. We refer to this configuration as $A_1^{1,6}$. There are two other configurations sufficiently low in energy which may be occupied at room temperature or higher. Both, labeled as $A_2^{1,6}$ and $A_3^{1,6}$, look similar to H_2^* in silicon bulk investigated in Refs. [54–56]. In the $A_2^{1,6}$ configuration, the Si atom involved in the H_2^* unit is neighboring to the vacant site and in the $A_3^{1,6}$ configuration it is not. Table II shows the calculated LDA, PBE, and PBE0 energies for the $A_1^{1,6}$, $A_2^{1,6}$, and $A_3^{1,6}$ configurations, while Fig. 1 illustrates the atomic arrangement in the defects.

B. V_2H_8 (H_2@V_2H_6)

It is known that monovacancies aggregate and form multivacancies. This is confirmed both from experiments [57,58] and theoretical studies [30]. In fact, first-principle calculations [30] show that the structures of m vacancies ($m \geqslant 3$) reconstruct in order to form fourfold coordinated structures with no dangling bonds. This is due to the fact that the energy gain by bond formation exceeds the strain energy associated with the distortion of atoms (in the proximity of multivacancies) from their bulk positions. It is also believed that if the dangling bonds created by removal of Si atoms are passivated by H atoms with sufficiently high hydrogen concentration, the aforementioned reconstruction does not happen.

TABLE II. Energies, in eV, of the three lowest energy configurations of VH_6, calculated with conventional exchange-correlation functionals (LDA and PBE) as well as a hybrid functional (PBE0). These are only DFT total energies, without zero point energies or any contribution from entropy at finite temperature.

XC functional	$A_1^{1,6}$	$A_2^{1,6}$	$A_3^{1,6}$
LDA	0.0	0.175	0.175
PBE	0.0	0.149	0.163
PBE0	0.0	0.087	0.103

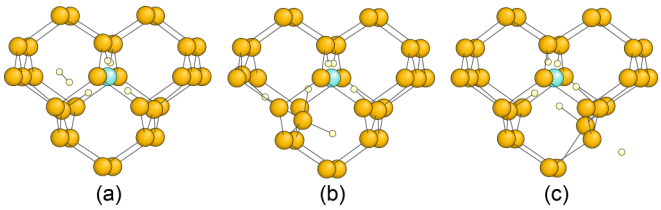

FIG. 1. (Color online) The three configurations of the 1 vacancy listed in Table II: (a) $A_1^{1,6}$, (b) $A_2^{1,6}$, (c) $A_3^{1,6}$. Si atoms (large spheres) are shown in orange, H atoms (small spheres) in yellow, and vacancies in blue. All other figures follow the same scheme.

Even though the stability of hydrogenated multivacancies has not been investigated in a systematic and complete way, it is believed that they aggregate as pure silicon vacancies do. In contrast to pure silicon vacancies which reconstruct to fourfold coordinated defects, hydogenation leads to intact vacant sites with H atoms terminating the dangling bonds to a varying extent. The 2 vacancy is the smallest system to examine the thermodynamic stability of aggregated hydrogenated silicon vacancies.

Our global optimization calculations show that, unlike pure silicon vacancies, hydrogenated silicon divacancies are thermodynamically less favorable than dissociated (split) hydrogenated vacancies. This conclusion remains unchanged if zero point energies (ZPEs) are included and it is true for deuterated 2 vacancies as well. More precisely, at least two extra H atoms must be present to passivate the greater number of dangling bonds due to the dissociation of a divacancy. In the case of a fully hydrogenated divacancy, namely V_2H_6, introduction of two H atoms is sufficient to passivate the extra two dangling bonds created by the dissociation of the divacancy.

Our result for 2 vacancy is as follows: We found two configurations that are appreciably lower in energy than the rest. In one of them [labeled $A_1^{2,8}$ shown in Fig. 2(b)], molecular H_2 is associated with a divacancy. The lowest energy configuration [split $S_1^{2,8}$ shown in Fig. 2(a)] consists

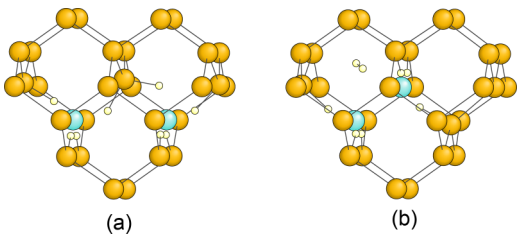

FIG. 2. (Color online) (a) The structure $S_1^{2,8}$. The monovacancies are second nearest neighbors and are connected by SiH_2. (b) The structure $A_1^{2,8}$. H_2 is at the T_d site dislodged towards the divacancy between two neighboring (001) planes. The H_2 is along [010] with bond length of 0.747 Å.

TABLE III. Energies, in eV, of the two lowest energy configurations of V_2H_8.

XC functional	$S_1^{2,8}$	$A_1^{2,8}$
LDA	0.0	0.053
PBE	0.0	0.042
PBE0	0.0	0.153

of two nearby fully hydrogenated monovacancies, VH_4. These two monovacancies in the structure $S_1^{2,8}$ are second nearest neighbors in the silicon lattice. In fact, higher energy configuration can be formed if VH_4 are further distant, i.e., third nearest neighbor, etc. The Si-H bonds in the SiH_2 unit which is connecting these two monovacancies, are rotated in the plane V-Si-V such that they break the symmetry and Si-H bonds do not point at the monovacancies. This introduces an additional term in the configurational entropy which makes this defect even more likely at finite temperatures. Using the enhanced splined saddle method [59], we calculated the energy barrier which separates these two symmetrically identical configurations. The barrier height is 0.138 eV at the LDA level. Such a low-energy barrier can be thermally surmounted readily in less than a nanosecond at room temperature.

Splitting the divacancy into two hydrogenated monovacancies was previously studied by Reboredo and coworkers [60]. They found that V_2H_8 splits into two hydrogenated monovacancies with an energy release of 0.1 eV, however, their calculations were much less rigorous than ours. In fact they did not perform a systematic search for the configurations but relied on an educated guess. Furthermore, the calculations were performed with 32- and 64-atom supercells which give rise to significant defect-defect interactions in m-vacancy systems with $m \geqslant 2$. Moreover, the forces were loosely converged to only 0.1 eVÅ^{-1} which prevents a quantitative comparison. In addition, the vacancy and interstitial formation energy values given in their paper were 4.2 and 3.0 eV, whereas recent LDA calculations using tighter convergence criteria

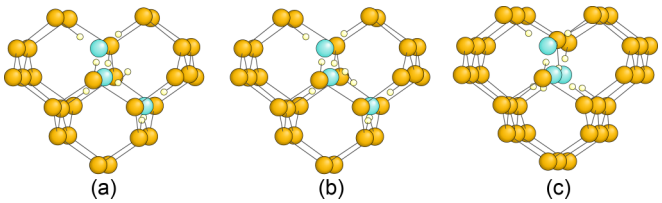

FIG. 4. (Color online) The three configurations of the 3 vacancies listed in Table IV: (a) $A_1^{3,10}$, (b) $A_2^{3,10}$, (c) $S_1^{3,10}$.

result in 3.5 [61] and 3.3 eV [62], respectively. It appears unlikely that a firm conclusion of whether the divacancy splits into monovacancies could have been drawn from their calculations. Table III shows the calculated LDA, PBE, and PBE0 energies for $S_1^{2,8}$ and $A_1^{2,8}$ configurations.

In 2001, Zhang [13] and Branz studied the ejection of a monovacancy from a multivacancy, in which the structure of the ejected monovacancy [Fig. 2(b) of Ref. [13]] is in agreement with our $S_1^{2,8}$ structure. They used H-atom energies as the reference energy in order to obtain binding energies of H atoms in a hydrogenated multivacancy. Therefore, one cannot deduce the relative stability between $S_1^{2,8}$ and $A_1^{2,8}$ from their results.

Zero-point energy can be of importance if light elements such as hydrogen are involved. Furthermore, in the case where potential energy differences are small, finite temperature contributions to the free energy cannot be neglected, in particular if there exist some low-frequency modes in one of the configurations. In order to account for the vibrational contributions to the free energy we rigorously calculate the complete phonon spectrum by employing the linear response technique as implemented in CPMD. Such calculations with hybrid functionals (namely PBE0) would require an enormous amount of computer resources. Therefore, we used PBE0 potential energy values but limited ourselves to employing the LDA exchange correlation functional for free energy and ZPE contributions. A detailed description on how to derive the

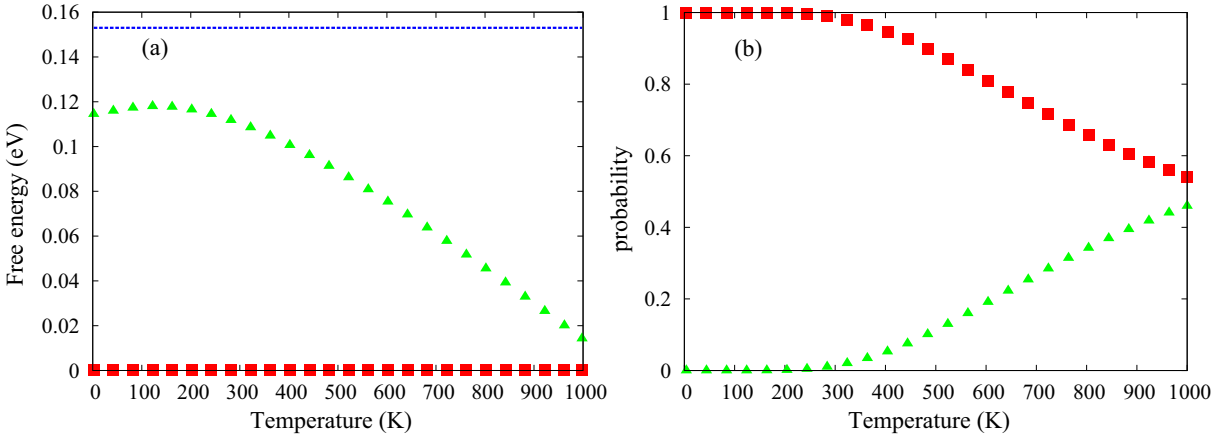

FIG. 3. (Color online) (a) The free energy, which includes the potential energy, the ZPE, as well as vibrational and configurational contributions to the entropy, is illustrated for the two lowest energy configurations in the case of the 2 vacancy (V_2H_8). The free energies are plotted relative to that of configuration $S_1^{2,8}$ at each temperature. The free energies of configurations $S_1^{2,8}$ and $A_1^{2,8}$ are shown by squares (red) and triangles (green), respectively. The solid line (blue) is the potential energy of configuration $A_1^{2,8}$ relative to that of $S_1^{2,8}$. (b) The normalized Boltzmann occupations are illustrated as a function of temperature for the configurations $S_1^{2,8}$ and $A_1^{2,8}$ by squares (red) and triangles (green), respectively.

TABLE IV. Energies, in eV, of the three lowest energy configurations of V_3H_{10}.

XC functional	$S_1^{3,10}$	$A_1^{3,10}$	$A_2^{3,10}$
LDA	0.0	0.008	0.012
PBE	0.0	−0.044	−0.044
PBE0	0.0	0.025	.025

free energy contribution from the vibrational partition function is given in Ref. [63]. Calculation of the full Hessian matrix is required in order to include free energy contributions from all modes. We find that this is important in calculating accurate the free energy and ZPE contributions. Figure 3 illustrates the free energies of the two configurations $S_1^{2,8}$ and $A_1^{2,8}$ at finite temperature. In addition, configurational entropy should also be included when calculating the free energy. This is taken into account in the finite temperature contribution for the $S_1^{2,8}$ configuration since two identical configurations of type $S_1^{2,8}$ are possible. As can be seen from Fig. 3, the ZPE contribution favors the $A_1^{2,8}$ configuration even though it embodies the H_2 molecule. However, this effect is not sufficient to make $A_1^{2,8}$ as low in energy as $S_1^{2,8}$. Therefore, at low temperatures, $S_1^{2,8}$ is dominantly populated. The free energy contribution from vibrational modes also favors the $A_1^{2,8}$ configuration over $S_1^{2,8}$ at high temperatures. However, below room temperature, its effect is negligible and $S_1^{2,8}$ remains as the dominant configuration if kinetics do not prevent conversion of $A_1^{2,8}$ to $S_1^{2,8}$. In fact, it is possible that $A_1^{2,8}$ would remain after quenching from a higher temperature.

In some experiments, silicon samples are treated by deuterium rather than hydrogen. We therefore replaced all H atoms by D and re-evaluated the ZPE and free energy contributions. The effect is negligible showing that contribution from the silicon lattice is larger than that of hydrogen or deuterium.

Finite temperature contributions of H_2 to the free energy in silicon bulk have previously been studied by Sanati and Estreivher [64]. In agreement with our results, they also concluded that finite temperature effects are significant although they did not have vacancies in their system.

C. V_3H_{10} (H_2@V_3H_8)

A 3 vacancy requires at least eight H atoms to fully saturate the dangling bonds due to silicon vacancies. We found three configurations which are energetically competitive. In two of them [Figs. 4(a) and 4(b)] the three vacant sites form a trimer, known as trivacancy. In the third shown in Fig. 4(c), one of the vacant sites is a second nearest neighbor to the divacancy. All three vacant sites in all three configurations lie in plane (110). The two trivacancy configurations are very similar and a H_2 molecule is trapped in the middle of the two most distant vacant sites. The only difference is the orientation of the H_2 molecule. In one configuration ($A_2^{3,10}$) it lies in the (110) plane and along the line connecting the two distant vacant sites. In the other configuration ($A_1^{3,10}$), the H_2 molecule is orthogonal to the plane of the trivacancy. The energy difference between these two configurations is less than the error in our calculations and they can be considered as degenerate states at the PBE0 level.

The calculated LDA, PBE, and PBE0 energies of these three configurations are shown in Table IV. The average SiH bond length is 1.48 Å and the H_2 bond length is 0.74 Å for both the $A_1^{3,10}$ and $A_2^{3,10}$ configurations in PBE0. In the third configuration ($S_1^{3,10}$), the trivacancy splits into a monovacancy and a divacancy which both lie in the (110) plane. The Si atom, which separates the monovacancy and the divacancy, is saturated by two H atoms. The SiH_2 unit which lies in the same plane, i.e., (110), is tilted towards the divacancy. A similar structure, in which the SiH_2 is, however, tilted towards the monovacancy, is about 0.2 eV (within LDA) higher in energy. The average SiH bond length in $S_1^{3,10}$ is the same as $A_1^{3,10}$ and $A_2^{3,10}$. The $S_1^{3,10}$ configuration is the lowest energy structure and is lower than $A_1^{3,10}$ and $A_2^{3,10}$ by 25 meV.

D. V_4H_{12} (H_2@V_4H_{10})

A 4 vacancy requires at least 10 H atoms to fully saturate the dangling bonds due to silicon vacancies. We found five configurations which are energetically competitive. In two of them [$A_1^{4,12}$ and $A_2^{4,12}$ shown in Figs. 5(a) and 5(b), respectively] the four vacant sites form a tetramer, known as tetravacancy. In the $A_1^{4,12}$ configuration, the vacant sites are a part-of-hexagonal ring (PHR) and in the $A_2^{4,12}$ configuration, the vacant sites form a trigonal pyramid. The additional H_2 is stabilized in both $A_1^{4,12}$ and $A_2^{4,12}$. In $A_2^{4,12}$ it lies slightly below the base of the trigonal pyramid and in $A_1^{4,12}$, it lies at the center of the PHR.

The remaining three configurations are split multivacancies, labeled $S_1^{4,12}$, $S_2^{4,12}$, and $S_3^{4,12}$, are shown in Figs. 5(c), 5(d), and 5(e) respectively. Both the $S_1^{4,12}$ and $S_2^{4,12}$ configurations consist of two divacancies where in the latter they lie in one plane and in the former they are in different planes. In both the $S_1^{4,12}$ and $S_2^{4,12}$ configurations, the two divacancies are separated by a SiH_2 unit. In $S_2^{4,12}$, the SiH_2 unit lies in the same plane as the two divacancies whereas in $S_1^{4,12}$, this is true only for one of the two divacancies. In $S_1^{4,12}$, the SiH_2 unit is tilted towards the divacancy which is in the plane. In

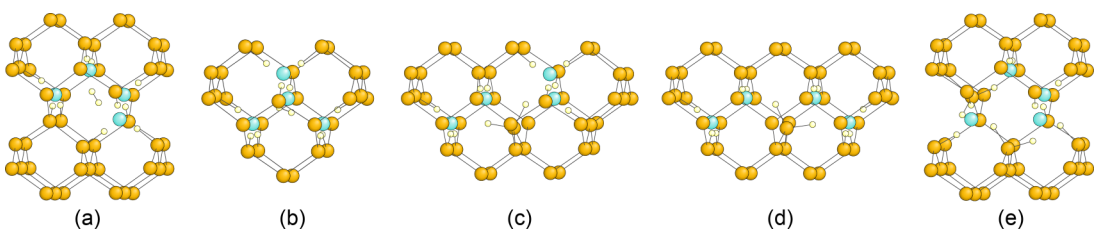

FIG. 5. (Color online) The five configurations of the 4 vacancies listed in Table V: (a) $A_1^{4,12}$, (b) $A_2^{4,12}$, (c) $S_1^{4,12}$, (d) $S_2^{4,12}$, (e) $S_3^{4,12}$.

TABLE V. Energies, in eV, of the five lowest energy configurations of V_4H_{12}.

XC functional	$A_1^{4,12}$	$A_2^{4,12}$	$S_1^{4,12}$	$S_2^{4,12}$	$S_3^{4,12}$
LDA	0.0	0.056	0.037	0.095	0.253
PBE	0.0	0.039	0.101	0.162	0.360
PBE0	0.0	0.007	0.034	0.088	0.302

TABLE VI. Energies, in eV, of the five lowest energy configurations of V_5H_{14}.

XC functional	$S_1^{5,14}$	$A_1^{5,14}$	$A_2^{5,14}$	$A_3^{5,14}$	$A_4^{5,14}$
LDA	0.0	0.077	0.119	0.127	0.156
PBE	0.0	−0.024	0.024	0.042	0.065
PBE0	0.0	0.046	0.075	0.103	0.132

$S_2^{4,12}$, tilting towards either of the divacancies results in exactly the same configuration due to symmetry. This configurational entropy would be taken into account if finite temperature effects are considered. In $S_3^{4,12}$, the 4 vacancy is split into one monovacancy and one trivacancy. Both are part of a hexagonal ring separated by two SiH_2 units, one tilted towards the monovacancy and the other towards the trivacancy. Again, due to symmetry, the two SiH_2 units can be tilted conversely which would be accounted for in finite temperature analysis. All these five configurations are depicted in Fig. 5.

The energy difference between $A_1^{4,12}$ and $A_2^{4,12}$ is less than our error and they can be considered as the lowest state at the PBE0 level. Since the $S_1^{4,12}$ and $S_2^{4,12}$ configurations are higher than $A_1^{4,12}$ and $A_2^{4,12}$ in energy by less than 0.1 eV, they can be partially populated at room temperature and above. However, the ZPEs and entropic contributions to the free energy can additionally favor $A_1^{4,12}$ and $A_2^{4,12}$ if V_4H_{12} behaves similarly to V_2H_8. The energetics for the 4-vacancy configurations show that splitting the tetravacancy into two divacancies is much more favorable than splitting it into a monovacancy and a trivacancy. Table V shows the calculated LDA, PBE, and PBE0 energies for all the *S*-type and *A*-type 4-vacancy configurations.

E. V_5H_{14} ($H_2@V_5H_{12}$)

A 5 vacancy requires at least 12 H atoms to fully saturate the dangling bonds due to silicon vacancies. We found five configurations which are energetically competitive. In four of them [$A_1^{5,14}$, $A_2^{5,14}$, $A_3^{5,14}$, and $A_4^{5,14}$ shown in Figs. 6(b), 6(c), 6(d), and 6(e) respectively] the five vacant sites form a pentamer, known as pentavacancy. In $A_1^{5,14}$, the vacant sites are a part of a hexagonal ring and the additional H_2 lies near the center of the pentavacancy. In $A_2^{5,14}$, four of the vacant sites lie in a hexagonal ring and the fifth one is attached to either of the center vacant sites perpendicular to the plane of the hexagonal ring. The additional H_2 is dislodged from the center of the vacancy PHR towards the vacant site which is outside the vacancy PHR plane. In $A_3^{5,14}$, four of the vacant sites lie in a hexagonal ring and the fifth one is attached to either of the ending vacant sites of the PHR while it is in the PHR plane. $A_4^{5,14}$ is similar to $A_2^{5,14}$ except the fifth vacant site is attached to either of the ending vacant sites.

In $S_1^{5,14}$ which is shown in Fig. 6(a), the 5 vacancy is split into one trivacancy and one divacancy. They are separated by two SiH_2 units, both tilted towards the divacancy. The trivacancy, divacancy, and the two SiH_2 units, are approximately in the (111) plane. The calculated LDA, PBE, and PBE0 energies for the aforementioned configurations are given in Table VI.

F. V_6H_{16} ($2H_2@V_6H_{12}$)

V_6H_{12} is a closed ring and it requires at least two additional H_2 to form an *S*-type configuration. Here we list the 10 lowest configurations from our calculations. Three are associate closed-ring structures (A' type), three are split (*S* type), and four are associate open ring (broken ring labeled as *A* type).

Even though two H_2 are present for the fully saturated V_6H_{12}, the first and second energetically lowest configurations are associate closed rings, $A_1'^{6,16}$ and $A_2'^{6,16}$, shown in Figs. 7(a) and 7(b), respectively. The two H_2 in $A_1'^{6,16}$ lie inside the hexavacancy and both are aligned such that they are perpendicular to the plane going through the hexavacancy. In $A_2'^{6,16}$, one of the H_2 remains inside the hexavacancy where the other one lies outside in vicinity of the hexavacancy. $A_3'^{6,16}$ (the 10th lowest), shown in Fig. 7(j), is similar to $A_2'^{6,16}$. However, the second H_2 is well outside the hexavacancy.

The third lowest configuration [$S_1^{6,16}$ shown in Fig. 7(c)] is a split configuration in which a vacancy is liberated from the hexavacancy and remains neighboring to it while separated by a SiH_3 unit. The former unit is rotated by 60° such that each H is pointing away from a vacant site. $S_2^{6,16}$, which is shown in Fig. 7(d), is similar to $S_1^{6,16}$ with the difference that the H atoms in the SiH_3 unit point to the vacant site and the unit is significantly moved towards the PHR center. In $S_3^{6,16}$ [the sixth lowest which is shown in Fig. 7(f)], a divacancy is ejected from the hexavacancy and it is separated by two SiH_2 units. The divacancy is in the same plane as the tetravacancy.

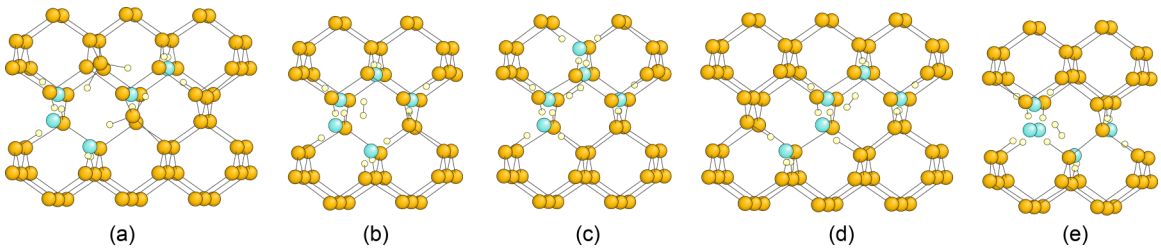

FIG. 6. (Color online) The five configurations of the 5 vacancies listed in Table VI: (a) $S_1^{5,14}$, (b) $A_1^{5,14}$, (c) $A_2^{5,14}$, (d) $A_3^{5,14}$, (e) $A_4^{5,14}$.

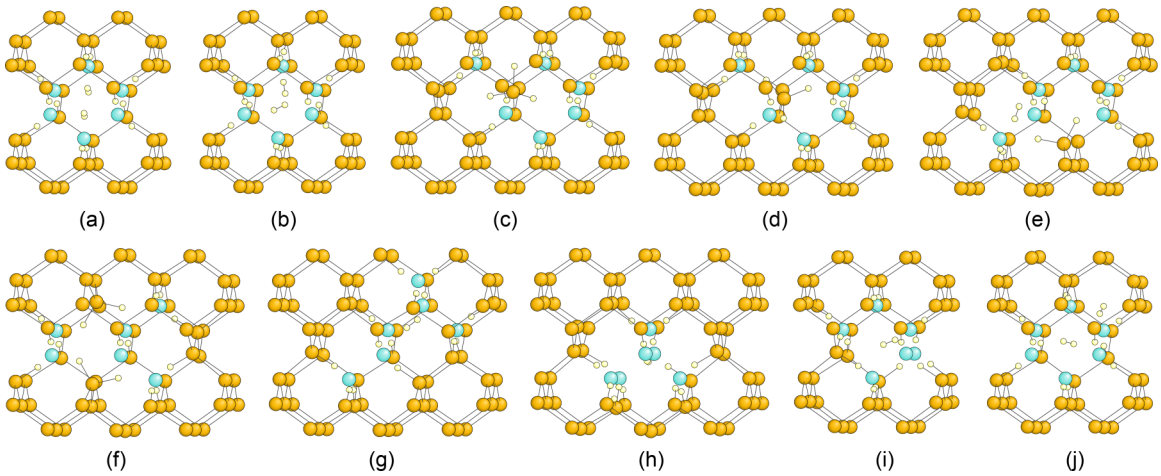

FIG. 7. (Color online) The 10 configurations of the 6 vacancies listed in Table VII are illustrated: (a) $A_1'^{6,16}$, (b) $A_2'^{6,16}$, (c) $S_1^{6,16}$, (d) $S_2^{6,16}$, (e) $A_1^{6,16}$, (f) $S_3^{6,16}$, (g) $A_2^{6,16}$, (h) $A_3^{6,16}$, (i) $A_4^{6,16}$, (j) $A_3'^{6,16}$.

The fifth lowest configuration [$A_1^{6,16}$ shown in Fig. 7(e)] is an associate configuration but is an open ring. Since the lowest energy configuration is of A' type, one might expect the A-type configuration to be the configuration next higher in energy. However, our lowest A type ($A_1^{6,16}$) is higher in energy than both $S_1^{6,16}$ and $S_2^{6,16}$. In $A_1^{6,16}$, the hexavacancy remains in one plane where the breaking vacancy comprises the tail of PHR. A SiH_2 unit is tilted towards the tail of the hexavacancy and the H_2 molecule lies on the other side of the tail. In $A_2^{6,16}$ shown in Fig. 7(g), the multivacancy is a (110) chain comprising four vacancies and the two other vacancies attached to its tail. There is no SiH_2 in this configuration and the remaining H_2 is along the chain located near its tail. In $A_3^{6,16}$ shown in Fig. 7(h), the breaking vacancy is attached to the second vacant site of the five-membered PHR and the SiH_2 unit is tilted towards its side of the ring. The remaining H_2 lies slightly above the PHR towards the breaking vacancy. In $A_4^{6,16}$ shown in Fig. 7(i), the breaking vacancy is connected to the middle vacant site of PHR and off the plane. The remaining H_2 is lifted up towards the breaking vacancy. The SiH_2 is not rotated and each H points towards the ending vacant site of the PHR. Table VII shows the calculated LDA, PBE, and PBE0 energies for all A'-type, A-type, and S-type configurations.

G. V_6H_{18} ($3H_2@V_6H_{12}$)

Stability of hexavacancy is expected due to its closed-ring structure. However, further insertion of hydrogen into hexavacancy may make it less stable such that A-type and eventually S-type configurations become energetically favorable. To examine this point, we study $3H_2@V_6H_{12}$ system. The lowest energy configuration is an associate open ring, labeled as $A_1^{6,18}$ and shown in Fig. 8(a), in which the breaking vacancy is attached to the end of the five-membered ring where it remains in the same plane as well. The two remaining H_2 molecules are each inside the PHR and outside in proximity of the breaking vacancy. The SiH_2 is tilted towards the breaking vacancy. This configuration is similar to $A_1^{6,16}$ with one additional H_2, indicating that this arrangement of vacant sites in the 6 vacancy is the most favorable among all associate open-ring configurations. The second lowest configuration [$A_2^{6,18}$ shown in Fig. 8(b)] is also an associate open ring. $A_2^{6,18}$ can be characterized as two four-membered vacancy rings which lie in orthogonal planes and share two vacancies. The two shared vacancies are the middle vacant sites and in the other one they are the ending vacant sites of the four-membered vacancy ring. There are no SiH_2 nor SiH_3 units in this configuration. The two H_2 molecules lie in the middle of each four-membered vacancy ring. $A_3^{6,18}$, which is shown in Fig. 8(d), is similar to the configuration $A_4^{6,16}$ with one additional H_2. However, another way of looking at this structure is as follows: The configuration is made up of two four-membered vacancy rings which share two vacancies both at their ending parts. The two remaining H_2 molecules each lie in the plane of a four-membered vacancy ring. The SiH_2 is tilted towards the four-membered vacancy ring which is not in the plane of a SiH_2 unit.

The third lowest [$S_1^{6,18}$ shown in Fig. 8(c)] is a split configuration in which a vacancy is liberated from the hexavacancy and remains neighboring to it while separated by a SiH_3 unit. The former unit is rotated by 60° such that each H is pointing away from the vacant site. The remaining H_2 lies inside the five-membered vacancy ring. This is indeed similar to configuration $S_1^{6,16}$ with one additional H_2.

TABLE VII. Energies, in eV, of the 10 lowest energy configurations of V_6H_{16}.

XC functional	$A_1'^{6,16}$	$A_2'^{6,16}$	$S_1^{6,16}$	$S_2^{6,16}$	$A_1^{6,16}$	$S_3^{6,16}$	$A_2^{6,16}$	$A_3^{6,16}$	$A_4^{6,16}$	$A_3'^{6,16}$
LDA	0.0	−0.022	0.077	0.145	0.075	0.118	0.170	0.143	0.153	0.073
PBE	0.0	0.014	0.205	0.261	0.202	0.264	0.217	0.206	0.207	0.152
PBE0	0.0	0.024	0.046	0.094	0.118	0.120	0.121	0.128	0.132	0.180

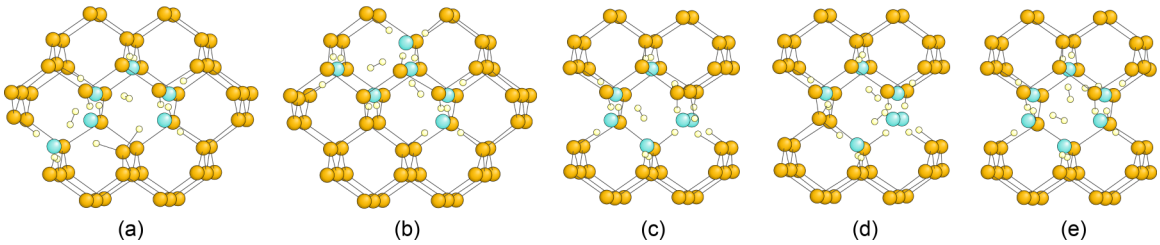

FIG. 8. (Color online) The five configurations of the 6 vacancies listed in Table VIII are illustrated: (a) $A_1^{6,18}$, (b) $A_2^{6,18}$, (c) $S_1^{6,18}$, (d) $A_3^{6,18}$, (e) $A_1'^{6,18}$.

The fifth lowest configuration, labeled as $A_1'^{6,18}$ and shown in Fig. 8(e), is an associate closed ring. One of the three H_2 molecules lies in the hexavacancy plane. The two remaining H_2 molecules lie above and below the plane. The calculated LDA, PBE, and PBE0 energies for the aforementioned configurations are given in Table VIII.

IV. VIBRATIONAL ANALYSIS

There are three vibrational frequencies observed experimentally in IR [15,22–25] and Raman spectroscopy [16,19,20] that are associated with H_2 in silicon. Mode 4158 cm^{-1} [namely H_2(I)] is attributed to H_2 in platelets. The value 4158 cm^{-1} is very close to H_2 in gaseous state (or in vacuum), i.e., 4161 cm^{-1} (see Refs. [65,66]). This assignment is plausible since any interactions between a H_2 molecule and its surroundings in platelets is negligible. A lower frequency is also observed by IR [22–26] (3618 cm^{-1}) and Raman spectroscopy [16,19] (3601 cm^{-1}), which are both denoted as H_2(II). The Raman peak at 3601 cm^{-1} approaches to a value of 3618 cm^{-1} as temperature decreases confirming these two modes belong to the same defect [16]. This mode is attributed to H_2 in bulk silicon at the T_d site. Reduction of the vibrational frequency of H_2 in bulk silicon from that of the gaseous state is due to the sizable interaction between the H_2 and its surroundings. Later in 1999, Ishioka and coworkers [5] observed a new Raman line at 3822 cm^{-1} [namely H_2(III)] in silicon after Si^+ implantation followed by a hydrogen atom plasma treatment. They speculated that the H_2 is trapped in H-terminated multivacancies and/or interstitial complexes. Their observation motivated some more experimental [3,6–8] and also theoretical [9,10,12,29] studies to identify the structure of the defect responsible for this Raman line.

Assignments of modes 4158 cm^{-1} and 3618 cm^{-1} (or 3601 cm^{-1}) are well established. Based on theoretical calculations, the mode at 3822 cm^{-1} is assigned to H_2 trapped in a multivacancy [9,10,12,29] (more specifically to a divacancy), however, this assignment is arguable for reasons discussed in the following. Conventional functionals in DFT do not describe well the vibrational frequency of H_2 within harmonic approximation and consequently the anharmonic value. In fact, hybrid functionals improve the predictive power of DFT significantly. Another factor is the effect of basis set completeness which imposes the use of a systematically extendable basis set such as plane waves or wavelets to establish a reliable conclusion. In addition, anharmonicity is an indispensable part of an accurate calculation for the vibrational frequency of the H_2 stretching mode. All previous theoretical investigations on H_2 molecules in bulk silicon and defected silicon lack considering all above issues collectively. For H_2 in the gaseous state, we also examined the effect of pseudopotentials in comparison to the full-potential DFT calculation using the MADNESS code [67]. The approximation due to the use of pseudopotentials for free H_2 is negligible. Therefore, the previous assignment of mode 3822 cm^{-1} to a divacancy by theoretical means is disputable. Furthermore, recently an experimental study by Socher and coworkers [8] has questioned the assignment of the mode at 3822 cm^{-1} to voidlike defects in silicon.

TABLE VIII. Energies, in eV, of the five lowest energy configurations of V_6H_{18}.

XC functional	$A_1^{6,18}$	$A_2^{6,18}$	$S_1^{6,18}$	$A_3^{6,18}$	$A_1'^{6,18}$
LDA	0.0	0.112	0.175	0.201	0.165
PBE	0.0	0.091	0.187	0.204	0.125
PBE0	0.0	0.089	0.125	0.213	0.228

We use the BIGDFT code to calculate vibrational frequencies. It should be noted that the CPMD code is used only for full Hessian calculations using the linear response method which was used for free energy calculation in Sec. III B. However, the BIGDFT code with hybrid functional is used for an accurate evaluation of the H_2 stretching mode. In addition to the implemented conventional XC functionals, the BIGDFT code is linked to the libXC library [69], including hybrid functionals. As expected, the highest mode obtained from a full Hessian matrix is associated with the stretching mode of an H_2 molecule as the corresponding eigenvector is aligned with an H_2 molecule better than 99.98%. Results in Table IX show that one should take into account anharmonic effects and employ hybrid functionals in order to accurately calculate the vibrational frequency of free H_2. Moreover, effects from nonsystematic basis sets are discussed by Okamoto *et al.* [70].

Next we calculated the vibrational frequency of H_2 in bulk silicon at the T_d site, using the methodology described above. Our calculated value using PBE0 with anharmonic corrections is 3615 cm^{-1} which differs from the experimental value (i.e., 3618 cm^{-1} by IR and 3601 cm^{-1} by Raman spectroscopy) by less than 10 cm^{-1} which can be considered negligible. All previous theoretical calculations based on the plane-wave basis set using conventional functionals had an error larger than 140 cm^{-1}. Saito and coworkers [70] calculated the vibrational frequency of H_2 in bulk silicon at the T_d site using Hartree-Fock, MP2, and hybrid functionals including anharmonic corrections, however, their results have an error

TABLE IX. The vibrational frequency (cm^{-1}) of the free H_2 molecule (as in vacuum) calculated by DFT using LDA all electron (full potential) as well as pseudopotential with various XC functionals, and the configuration interaction (CI) method is presented. Both harmonic (ω_0) and anharmonic (ω) values are listed.

Method	ω_0	ω	$\omega - \omega_0$
LDA all electron	4180	3950	−230
LDA pseudopotential	4172	3941	−231
PBE	4309	4057	−252
PBE0	4399	4169	−230
CI[a]	4403	4150	−253
Expt.[b]	4400	4161	−239

[a]CI values are derived based on paper by Schwenke [68].
[b]Refs. [65,66].

of about 400 cm^{-1} due to the nonsystematic basis set and the fact that they used H-terminated small silicon clusters instead of silicon bulk. Table X shows the vibrational frequency of an H_2 molecule in bulk silicon at the T_d site and in silicon 1, 2, and 3 vacancies, respectively. These results indicate an increase of vibrational frequency as the size of multivacancy increases. The lowest vibrational frequency belongs to H_2 in bulk (no vacancy) at the T_d site and eventually at trivacancy it reaches that of free H_2 (gaseous state). The Raman peak at 3822 cm^{-1} was previously expected to belong to an H_2 trapped in this range of vacancy size, however, our calculations do not show any mode close to 3822 cm^{-1}.

Due to the fact that the ground state of V_2H_8 is a dissociated configuration, addition of an extra hydrogen molecule may be the defect which is responsible for the Raman peak at 3822 cm^{-1}. To examine this point, we added one H_2 to various empty sites in the $S_1^{2,8}$ structure, and calculated the vibrational frequencies. Among eight examined configurations, three are appreciably lower in energy than the rest. The second and third lowest configurations are 0.161 and 0.172 eV higher than the ground state in which the H_2 molecule is located in the plane of the SiH_2 unit and parallel to its two H atoms. The H_2 molecule is between the two vacant sites and above the line connecting them. In the second lowest energy configuration, the H_2 molecule is in the plane of the SiH_2 unit but not between the two vacant sites. In the third lowest energy configuration, the H_2 molecule is parallel to the plane of the SiH_2 unit and about 1.6 Å distant from the plane. The vibrational frequencies of H_2 in the three configurations are 4089 cm^{-1}, 3904 cm^{-1}, and 3941 cm^{-1}, respectively. Even though the smallest vibrational frequency, which belongs to the second lowest energy configuration, not the ground state, is about 80 cm^{-1} higher than 3822 cm^{-1}, and thus we do not expect any of these three defects to be responsible for the Raman peak at 3822 cm^{-1}.

TABLE X. The bond lengths (Å) and vibrational frequency (cm^{-1}) of an H_2 molecule in bulk silicon at the T_d site and in 1, 2, and 3 vacancies. These values are obtained using the PBE0 functional and include anharmonic corrections.

System	Bond length	ω_0	$\Delta\omega$	ω	ω (expt.)
H_2 at T_d Si Bulk	0.763	3951	−336	3615	3618
$A_1^{1,6}$	0.757	4057	−317	3740	
$A_1^{2,8}$	0.747	4262	−261	4001	
$A_1^{3,10}$	0.743	4405	−243	4162	
$A_2^{3,10}$	0.743	4403	−244	4159	

V. DISCUSSION

We have studied hydrogenated m vacancies ($m = 1, \ldots, 6$) in a systematic way by means of a global optimization method in which Si and H atoms are treated by a tight binding scheme. All global optimization runs as well as subsequent more accurate calculations using DFT with conventional and hybrid functionals are performed with a 216-atom supercell. Moreover, all other parameters in the calculations are chosen carefully to be converged in order to avoid any artifacts which may affect our analysis. The Lenosky silicon tight binding scheme is extended to include Si-H and H-H interactions, the parameters for which are listed in this paper. Our decision to employ the tight binding Hamiltonian for the global optimization simulations instead of more accurate DFT methods is based on the size of the system under investigation (circa 216 atoms). On the other hand, however, empirical force fields, which are in fact even faster than tight binding, are not viable due to their insufficient accuracy as shown in Ref. [37]. Our global optimization program [35,71] besides aiming at the global minimum, explores exhaustively the low-lying local minima. These low-lying energy configurations are then examined at a higher level of theory, namely DFT with conventional XC functionals. In the last step the PBE0 hybrid functional is used to obtain the putatively most accurate energies.

All systems studied here contain at least one additional H_2 molecule above full saturation. The results in Sec. III indicate that the H atoms form very strong bonds with the Si atoms which are neighbors to the vacancies. These bonds are so strong that they are responsible for the breakage of multivacancies into smaller vacancies. These new split configurations are favored for an m vacancy with $m = 2,3,5$ provided the hydrogen concentration is sufficiently large to terminate the additional dangling bonds. As the multivacancy grows, split configurations become less favorable and eventually for the hexavacancy, which is a closed ring, associate configurations are favored. In addition to SiH subunits, the split configurations of medium or larger size comprise SiH_2 units and to a smaller extent SiH_3 subunits.

The Raman peak at 3822 cm^{-1} originally observed by Ishioka [5] in Si^+-implanted samples treated by hydrogen plasma, has also been observed in proton-implanted samples, however, at slightly different frequency, namely 3810 cm^{-1}. The latter is of importance since it may be relevant to the technologically important Smart Cut process used commercially in the fabrication of thin silicon-on-insulator layers. Our result, i.e., the higher stability of S-type configurations compared to A-type configurations, is of particular interest for divacancies since the new Raman peak at 3822 cm^{-1} was previously assigned to an H_2 molecule trapped in such a divacancy. Therefore, we investigated the divacancy more carefully and considered ZPE and finite temperature effects. The ZPE could play a role due to light H atoms present in

the system and finite temperature effects could be significant because of vibrational entropy caused by weak interactions between the H_2 molecule and their surroundings.

Using linear response methods, the full second derivative matrix is evaluated and the the entire vibrational spectrum is used to assess the importance of ZPE. Due to the presence of H_2 molecules in A-type configurations, one may expect that the $A_1^{2,8}$ configuration to be disfavored over $S_1^{2,8}$ with respect to ZPE. Surprisingly, our calculation shows that the ZPE changes the energy difference by about 40 meV in favor of $A_1^{2,8}$, although the potential energy of $S_1^{2,8}$ including ZPE remains lower. As expected, the finite temperature effects favor the $A_1^{2,8}$ configuration over $S_1^{2,8}$ due to low frequencies associated with the rotation of H_2. Figure 3 shows the free energy of $A_1^{2,8}$ and $S_1^{2,8}$ for the temperature range which experiments probed for these systems. Based on these results $S_1^{2,8}$ is favored even at high temperature, although $A_1^{2,8}$ will be significantly populated at high temperatures. Furthermore, results by Mori [6,7] and coworkers show that the Raman peak at 3822 cm^{-1} disappears at high temperatures. This is expected since due to the entropic effects H_2 molecules favor leaving the silicon system at high temperatures and kinetics cannot prevent the process at such temperatures. Therefore, we conclude that in the presence of additional H_2, V_2H_6 splits into two VH_4 and the Raman peak at 3822 cm^{-1} is not associated with a H_2 trapped in a fully hydrogenated divacancy.

In order to assess this claim more carefully, we accurately calculated the vibrational frequency of H_2 using the PBE0 functional and including anharmonic effects which are both essential for a precise investigation of the vibrational frequency of H_2. The well-known self-interaction error in conventional functionals is of great importance for H_2 and it has been shown that the use of hybrid functionals can alleviate this to a large extent. Similar to previous studies, our results indicate that anharmonic effects are of importance, independent of the choice of the XC functional. Moreover, the fact that we used a code based on a systematic basis set (BIGDFT) eliminates the errors which may arise from incomplete basis sets. In this way we are able to obtain results which have a higher predictive power than previously published results for the vibrational frequency of free H_2 and that of H_2 in bulk silicon at T_d sites. We then exploit the same procedure for calculations involving H_2 molecules trapped in fully hydrogenated silicon multivacancies. Our results show that there is no vibrational frequency near 3822 cm^{-1} for H_2 molecules trapped in mono-, di- or trivacancies. It is worth mentioning that the vibrational frequency of H_2 increases in larger multivacancies. Therefore we do not expect the Raman peak at 3822 cm^{-1} to belong to a H_2 trapped in multivacancies larger than trivacancy as well. However, we do not exclude the possibility of some nontrivial S-type configurations of m vacancy ($m > 3$) with sufficiently large H_2 concentration to be responsible for the Raman peak at 3822 cm^{-1}. In agreement with our results for energetics of the 2 vacancy, the vibrational frequency analysis confirms as well our claim that 3822 cm^{-1} does not belong to a H_2 trapped in a divacancy in contrast to previous theoretical studies.

ACKNOWLEDGMENTS

Financial support was provided by the Swiss National Science Foundation (SNSF). The calculations were done at the Swiss National Supercomputing center CSCS in Lugano.

[1] J. I. Pankove and N. M. Johnson, *Hydrogen in Semiconductors, in Semiconductors and Semimetals* (Academic Press, Boston, 1991), Vol. 34.
[2] M. Bruel, Electron. Lett. **31**, 1201 (1995).
[3] J. Weber, T. Fischer, E. Hieckmann, M. Hiller, and E. V. Lavrov, J. Phys.: Condens. Matter **17**, S2303 (2005).
[4] Y. J. Chabal, M. K. Weldon, Y. Caudano, B. B. Stefanov, and K. Raghavachari, Physica B **273**, 152 (1999).
[5] K. Ishioka, M. Kitajima, S. Tateishi, K. Nakanoya, N. Fukata, T. Mori, K. Murakami, and S. Hishita, Phys. Rev. B **60**, 10852 (1999).
[6] T. Mori, K. Otsuka, N. Umehara, K. Ishioka, M. Kitajima, S. Hishita, and K. Murakami, Physica B **302**, 239 (2001).
[7] T. Mori, K. Otsuka, N. Umehara, K. Ishioka, M. Kitajima, S. Hishita, and K. Murakami, Physica B **308**, 171 (2001).
[8] S. Socher, E. V. Lavrov, and J. Weber, Phys. Rev. B **86**, 125205 (2012).
[9] T. Akiyama, Y. Okamoto, M. Saito, and A. Oshiyama, Jpn. J. Appl. Phys. **38**, L1363 (1999).
[10] T. Akiyama and A. Oshiyama, Physica B **273**, 516 (1999).
[11] S. K. Estreicher, J. L. Hastings, and P. A. Fedders, Mater. Sci. Eng. B **58**, 31 (1999).
[12] M. Saito, Y. Okamoto, A. Oshiyama, and T. Akiyama, Physica B **273-274**, 196 (1999).
[13] S. B. Zhang and H. M. Branz, Phys. Rev. Lett. **87**, 105503 (2001).
[14] Y. S. Kim and K. J. Chang, Phys. Rev. Lett. **86**, 1773 (2001).
[15] K. Murakami, N. Fukata, S. Sasaki, K. Ishioka, M. Kitajima, S. Fujimura, J. Kikuchi, and H. Haneda, Phys. Rev. Lett. **77**, 3161 (1996).
[16] A. W. R. Leitch, V. Alex, and J. Weber, Phys. Rev. Lett. **81**, 421 (1998).
[17] B. Hourahine, R. Jones, S. Öberg, R. C. Newman, P. R. Briddon, and E. Roduner, Phys. Rev. B **57**, R12666 (1998).
[18] M. Hiller, E. V. Lavrov, and J. Weber, Phys. Rev. B **74**, 235214 (2006).
[19] M. Kitajima, K. Ishioka, K. Nakanoya, S. Tateishi, T. Mori, N. Fukata, K. Murakami, and S. ichi Hishita, Jpn. J. Appl. Phys. **38**, L691 (1999).
[20] K. Murakami, K. Ishioka, M. Kitajima, S. Tateishi, K. Nakanoya, T. Mori, and S. Hishita, Physica B **273**, 188 (1999).
[21] M. Hiller, E. V. Lavrov, and J. Weber, Phys. Rev. B **80**, 045306 (2009).
[22] R. E. Pritchard, M. J. Ashwin, J. H. Tucker, R. C. Newman, E. C. Lightowlers, M. J. Binns, S. A. McQuaid, and R. Falster, Phys. Rev. B **56**, 13118 (1997).
[23] R. E. Pritchard, M. J. Ashwin, J. H. Tucker, and R. C. Newman, Phys. Rev. B **57**, R15048 (1998).

[24] R. C. Newman, R. E. Pritchard, J. H. Tucker, and E. C. Lightowlers, Phys. Rev. B **60**, 12775 (1999).
[25] J. A. Zhou and M. Stavola, Phys. Rev. Lett. **83**, 1351 (1999).
[26] N. Fukata, T. Ohori, M. Suezawa, and H. Takahashi, J. Appl. Phys. **91**, 5831 (2002).
[27] Y. Okamoto, M. Saito, and A. Oshiyama, Phys. Rev. B **56**, R10016 (1997).
[28] C. G. Van de Walle, Phys. Rev. Lett. **80**, 2177 (1998).
[29] T. Akiyama and A. Oshiyama, J. Phys. Soc. Jpn. **70**, 1627 (2001).
[30] S. Lee and G. S. Hwang, Phys. Rev. B **78**, 125310 (2008).
[31] D. J. Chadi and K. J. Chang, Phys. Rev. B **38**, 1523 (1988).
[32] J. L. Hastings, S. K. Estreicher, and P. A. Fedders, Phys. Rev. B **56**, 10215 (1997).
[33] T. E. M. Staab, A. Sieck, M. Haugk, M. J. Puska, T. Frauenheim, and H. S. Leipner, Phys. Rev. B **65**, 115210 (2002).
[34] T. J. Lenosky, J. D. Kress, I. Kwon, A. F. Voter, B. Edwards, D. F. Richards, S. Yang, and J. B. Adams, Phys. Rev. B **55**, 1528 (1997).
[35] S. Goedecker, J. Chem. Phys. **120**, 9911 (2004).
[36] W. Hellmann, R. G. Hennig, S. Goedecker, C. J. Umrigar, B. Delley, and T. Lenosky, Phys. Rev. B **75**, 085411 (2007).
[37] S. A. Ghasemi, M. Amsler, R. G. Hennig, S. Roy, S. Goedecker, T. J. Lenosky, C. J. Umrigar, L. Genovese, T. Morishita, and K. Nishio, Phys. Rev. B **81**, 214107 (2010).
[38] J. M. Soler, E. Artacho, J. D. Gale, A. García, J. Junquera, P. Ordejón, and D. Sánchez-Portal, J. Phys.: Condens. Matter **14**, 2745 (2002).
[39] L. Genovese, A. Neelov, S. Goedecker, T. Deutsch, S. A. Ghasemi, A. Willand, D. Caliste, O. Zilberberg, M. Rayson, A. Bergman, and R. Schneider, J. Chem. Phys. **129**, 014109 (2008).
[40] C. Hartwigsen, S. Goedecker, and J. Hutter, Phys. Rev. B **58**, 3641 (1998).
[41] D. C. Allan and E. J. Mele, Phys. Rev. B **31**, 5565 (1985).
[42] B. J. Min, Y. H. Lee, C. Z. Wang, C. T. Chan, and K. M. Ho, Phys. Rev. B **45**, 6839 (1992).
[43] E. Kim, Y. H. Lee, and J. M. Lee, J. Phys.: Condens. Matter **6**, 9561 (1994).
[44] G. Panzarini and L. Colombo, Phys. Rev. Lett. **73**, 1636 (1994).
[45] Q. Li and R. Biswas, Phys. Rev. B **50**, 18090 (1994).
[46] D. R. Bowler, M. Fearn, C. M. Goringe, A. P. Horsfield, and D. G. Pettifor, J. Phys.: Condens. Matter **10**, 3719 (1998).
[47] N. C. Bacalis and A. D. Zdetsis, J. Math. Chem. **46**, 962 (2009).
[48] T. Frauenheim, F. Weich, T. Köhler, S. Uhlmann, D. Porezag, and G. Seifert, Phys. Rev. B **52**, 11492 (1995).
[49] D. Marx and J. Hutter, *Ab Initio Molecular Dynamics* (Cambridge University Press, Cambridge, 2009).
[50] M. J. D. Powell, Comput. J. **7**, 303 (1965).
[51] S. A. Ghasemi, S. Goedecker, A. Baratoff, T. Lenosky, E. Meyer, and H. J. Hug, Phys. Rev. Lett. **100**, 236106 (2008).
[52] P. Pou, S. A. Ghasemi, P. Jelinek, T. Lenosky, S. Goedecker, and R. Perez, Nanotechnology **20**, 264015 (2009).
[53] J. A. Flores-Livas, M. Amsler, T. J. Lenosky, L. Lehtovaara, S. Botti, M. A. L. Marques, and S. Goedecker, Phys. Rev. Lett. **108**, 117004 (2012).
[54] K. J. Chang and D. J. Chadi, Phys. Rev. B **40**, 11644 (1989).
[55] K. J. Chang and D. J. Chadi, Phys. Rev. Lett. **62**, 937 (1989).
[56] C. G. Van de Walle, Phys. Rev. B **49**, 4579 (1994).
[57] V. C. Venezia, D. J. Eaglesham, T. E. Haynes, A. Agarwal, D. C. Jacobson, H.-J. Gossmann, and F. H. Baumann, Appl. Phys. Lett. **73**, 2980 (1998).
[58] P. Mascher, S. Dannefaer, and D. Kerr, Phys. Rev. B **40**, 11764 (1989).
[59] S. A. Ghasemi and S. Goedecker, J. Chem. Phys. **135**, 014108 (2011).
[60] F. A. Reboredo, M. Ferconi, and S. T. Pantelides, Phys. Rev. Lett. **82**, 4870 (1999).
[61] A. F. Wright, Phys. Rev. B **74**, 165116 (2006).
[62] W. D. Parker, J. W. Wilkins, and R. G. Hennig, Physica Status Solidi b **248**, 267 (2011).
[63] J. W. Ochterski, *Thermochemistry in Gaussian* (Gaussian, Wallingford, 2000).
[64] M. Sanati and S. K. Estreicher, Solid State Commun. **128**, 181 (2003).
[65] K. Huber and G. Herzberg, *Molecular Spectra and Molecular Structure. IV. Constants of Diatomic Molecules* (Van Nostrand Reinhold, New York, 1979).
[66] B. P. Stoicheff, Can. J. Phys. **35**, 730 (1957).
[67] R. J. Harrison, G. I. Fann, T. Yanai, Z. Gan, and G. Beylkin, J. Chem. Phys. **121**, 11587 (2004).
[68] D. W. Schwenke, J. Chem. Phys. **89**, 2076 (1988).
[69] M. A. L. Marques, M. J. T. Oliveira, and T. Burnus, Comput. Phys. Commun. **183**, 2272 (2012).
[70] Y. Okamoto, M. Saito, and A. Oshiyama, Phys. Rev. B **58**, 7701 (1998).
[71] M. Amsler and S. Goedecker, J. Chem. Phys. **133**, 224104 (2010).